Investigation of Gravity-Driven Coastal Currents

Grégorio S.O.[1], Thomas P.J.[1], Linden P.F.[2], Levin J.C.[3]. Haidvogel D.B.[3], Taskinoglu E.S.[3]

[1] *University of Warwick, Fluid Dynamics Research Centre, Coventry CV4 7AL, United Kingdom*
[2] *University of California, Department of Mechanical and Aerospace Engineering, San Diego, USA*
[3] *Rutgers University, Institute of Marine and Coastal Sciences, 71 Dudley Road, New Brunswick, USA*
Email address of the corresponding author: S.Gregorio@warwick.ac.uk

Abstract :

We summarize a study that compares experimental laboratory data for gravity-driven coastal surface currents with corresponding theoretical results obtained from a new geostrophic model describing such currents. It is found that experiment and theory are, generally, in good agreement.

Key-words :

Gravity-Driven Flows; Rotating Flows; Coastal Currents

1 Introduction

When estuarine river water is discharged into the coastal zone, gravity-driven surface flows can be established (**?**). These flows develop as a consequence of the density difference between the buoyant estuarine fresh water and the denser, salty ocean water. For sufficiently large discharge rates, i.e. when the current exceeds length scales larger than the Rossby deformation scale, the current dynamics are affected by the Coriolis force arising from the rotation of the earth. As a result the discharged fresh water is confined to the coastal zone where it forms a current flowing along the coast.

? and, more recently, **?**, derived scaling relations for the current width, its depth and its velocity. However, since these relations were based on scaling arguments they did not yield the constants of proportionality missing from the expressions obtained. We derived a new analytical model which readily yields values for the constants. The expressions obtained are similar to those of **?**. Here we summarize how the predictions of our model compare to results from our laboratory experiments - for a detailed comparison, refer to **?**.

2 Experimental set-up

Two complementing sets of experiments, using different experimental facilities, were carried out. The two facilities had substantially different spatial scales enabling the investigation of a wide range of the independent experimental parameters. Small-scale laboratory experiments were performed on a rotating turntable supporting a fluid-filled tank with a radius of approximately 0.5m. Large-scale experiments were conducted at the *Coriolis Facility* (LEGI, Grenoble) where the rotating basin has a radius of 6.5m.

The principle of the experiments and the arrangement of the small-scale experimental facility are illustrated in Fig. 1. The tank was filled with salt water of density ρ_2 representing the ocean water. Fresh water of density ρ_1, with $\rho_1 < \rho_2$, was released from a small source mounted at the wall of the tank to simulate estuarine discharges. The source was adjusted to be level with the surface of the dense salt water. The fluid was discharged vertically upwards, rather than horizontally, as would be the case in the natural environment, in order to minimize

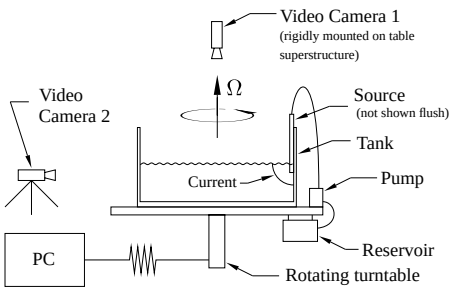

Figure 1: Small-scale setup.

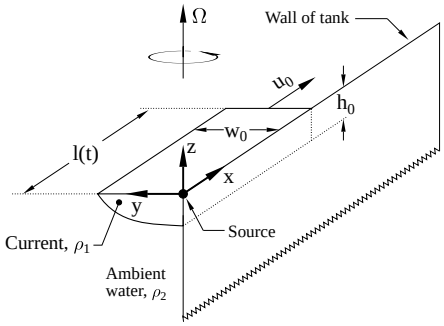

Figure 2: Nomenclature for model.

momentum-flux effects and mixing of fresh water and salt water near the source. Fluid was released continuously and with a constant volumetric discharge rate q_0. The density difference between the fresh water and the salt water is characterized in terms of the reduced gravity, g', defined by $g' = ((\rho_2 - \rho_1)/\rho_1)\, g$ with $g = 981$ cm s^{-2}. The rotation rate, Ω, of the turntable was constant for each experiment. The salt water inside the tank was in solid-body rotation prior to the start of fluid being released from the source. For visualization purposes the fresh water discharging at the source was dyed with food colouring while the ambient salt water was clear. The large-scale experiments were designed to mirror the small-scale study.

3 Theoretical description of the problem

Our model assumes that the flow velocities normal to the wall and in the vertical direction (see Fig. 2) are negligible in comparison to the along-wall flow velocity. We allow for motion along the $x-$axis but neglect all derivatives $\partial/\partial x$. We use the geostrophic approximation, assume that the potential vorticity is zero and conserved, and we also employ mass conservation. The final, main theoretical results of **?** are

$$h_0 = \left(\frac{4\Omega\, q_0}{g'}\right)^{\frac{1}{2}}, \quad w_0 = \left(\frac{g'\, q_0}{\Omega^3}\right)^{\frac{1}{4}}, \quad l(t) = \frac{3}{4}(q_0 g' \Omega)^{\frac{1}{4}} t, \tag{1}$$

where the meaning of h_0, w_0 and $l(t)$ is apparent from Fig. 2. The expressions in Eq. (1) can be conveniently expressed in dimensionless form. We use the non-dimensional time $T = \Omega t$ and non-dimensionalize lengths by $w_0 = (g' q_0/\Omega^3)^{1/4}$. Using capital letters to denote non-dimensional variables, one obtains

$$H_0 = \frac{h_0}{w_0} = 2I^{\frac{5}{4}}, \quad W = \frac{w_0}{w_0} = 1, \quad L = \frac{l(t)}{w_0} = \frac{3}{4}T \tag{2}$$

where $I = \Omega q_0^{1/5}/g'^{3/5}$ is a dimensionless parameter that describes the aspect ratio, h_0/w_0, of the current. For a detailed description of our model consult **?**.

4 Experimental results

4.1 Qualitative observations

Figure 3 shows a flow visualization illustrating a typical current observed in the small-scale facility for $I = 0.3264$. The picture shows a current viewed from above the circular tank,

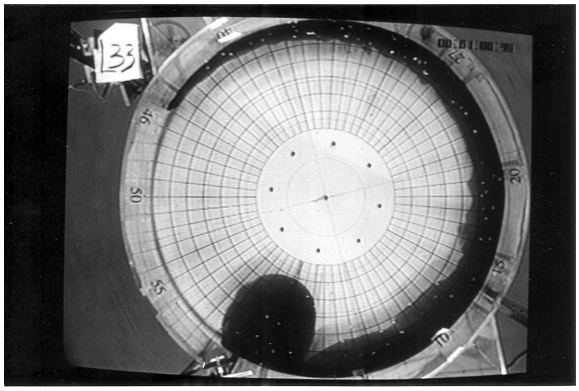

Figure 3: Current (dark fluid) flowing along the wall of the circular tank in the small-scale facility. Turntable rotates anti-clockwise, current also propagates anti-clockwise keeping wall to its right.

looking vertically downwards onto the fluid surface. The source outlet, where the buoyant current fluid is ejected, is located at the wall of the tank, just to the right of the anti-cyclonically (i.e. clockwise) spinning gyre which has developed in the vicinity of the source. As discussed in **?**, the large-scale currents observed in the *Coriolis Facility* look qualitatively very similar to those developing in the small-scale facility, but currents can appear quite different for different values of I.

4.2 Current length

Figures 4 and 5 display summaries of 66 small-scale experiments and the 34 large-scale experiments respectively. The figures display the non-dimensional current length, L, *vs.* non-dimensional time, T. The solid line superposed onto both figures represents the theoretical prediction $L = 3/4\,T$ from Eq. (2). Comparison of the two figures shows that they are very similar. In both cases experiment and theory are in good agreement. Inspection of Figs. 4 and 5 reveals that a superposition of the two figures collapses both data sets *onto* each other. Hence, the small-scale and large-scale experiments display corresponding dynamic behaviour. The dashed

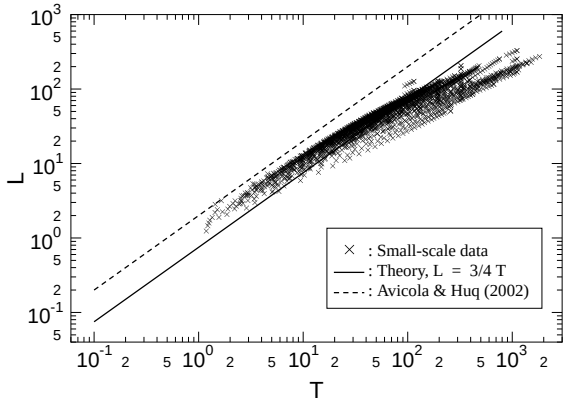

Figure 4: L *vs.* T; Small-scale data.

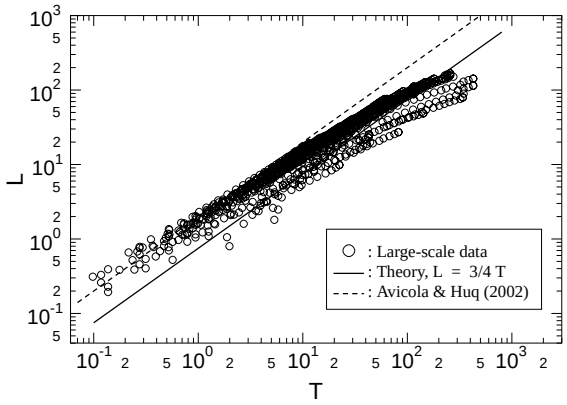

Figure 5: L *vs.* T; Large-scale data.

line superposed onto Figs. 4 and 5 represents the theoretical result of Avicola & Huq (2002) which is $L = 2T$ in our nomenclature (see **?**). Figure 4 shows that, for the small-scale exper-

iments, our model predicts the propagation of the current head overall slightly better than the model of Avicola & Huq. For the large-scale data the opposite seems to be the case. However, a detailed discussion, which is contained in **?**, concurrently needs to take the data for the depth into account. If this is done then the data analysis suggests that it is probably justified to concluded that, overall, the agreement between the experimental data in both the small-scale and the large-scale experiments, is in slightly better agreement with our present model than with the model of Avicola & Huq (2002).

4.3 Current height

According to our model, the current height, h_0, at the wall of the tank (see Fig. 2 and Eq. (1)) is constant, i.e. it is independent of the x-coordinate. However, the videos of the experiments reveal that the current height decreases between the source region and the current head. A sketch schematically illustrating the observed height profile at the wall ($y = 0$), in the x-z plane of Fig. 2, is shown in Fig. 6. The current has a maximum height, h_m in Fig. 6, just downstream

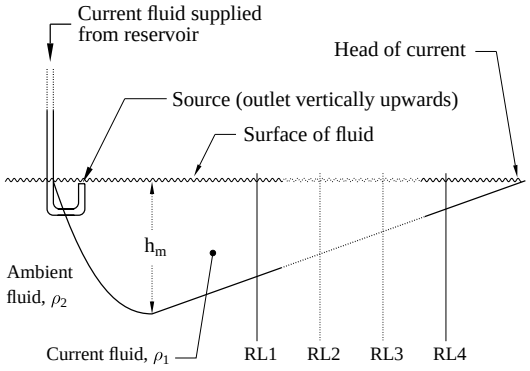

Figure 6: A side-view ($x - z$ plane in Fig. 2) of a current as recorded by Video Camera 2 shown in Fig. 1.

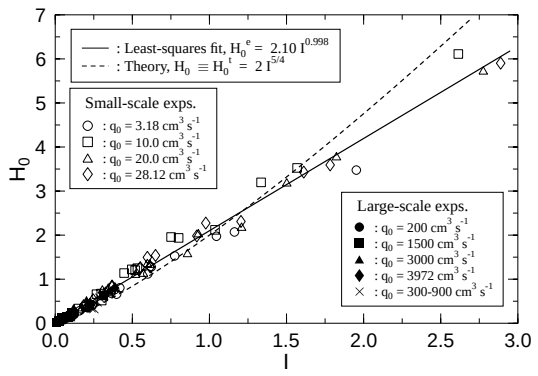

Figure 7: Non-dimensional maximum current height, $H_0 = h_m/w_0$, near the source as a function of I.

of the source. This height h_m was observed to be constant throughout each experiment. It was used for comparison with the theoretical prediction for h_0 of Eq. (1) *viz.* H_0 of Eq. (2).

Figure 7 summarizes the measured values for the non-dimensional height $H_0 = h_m/w_0$ as a function of I. A least squares fit interpolating all data points gives $H_0^e = 2.10I^{0.998}$ and is shown as the solid line in Fig. 7. The dashed line in Fig. 7 is the theoretical prediction $H_0 = 2I^{5/4}$. It can be seen that experiment and theory are overall in good agreement. A similarly good agreement is also found for the current width as is discussed in **?**.

5 Froude number

We calculate experimental values for the Froude number, $Fr(T_i) = \overline{u_0^e}/\sqrt{g'h_m}$, based on the measured current mean velocity $\overline{u_0^e} = l_i/t_i$ and the measured maximum depth h_m near the source. The results obtained in this way are displayed in Figs. 8 and 9. The two figures reveal that, for both our sets of experiments, the Froude number is in the range of approximately $0.1 \leq Fr \leq 1.51$ and the figures illustrate how Fr decreases with time, T.

In Figs. 8 and 9, the data points for the different runs have been grouped into three different sets according to their values of the parameter I. Both figures reveal that there is a general

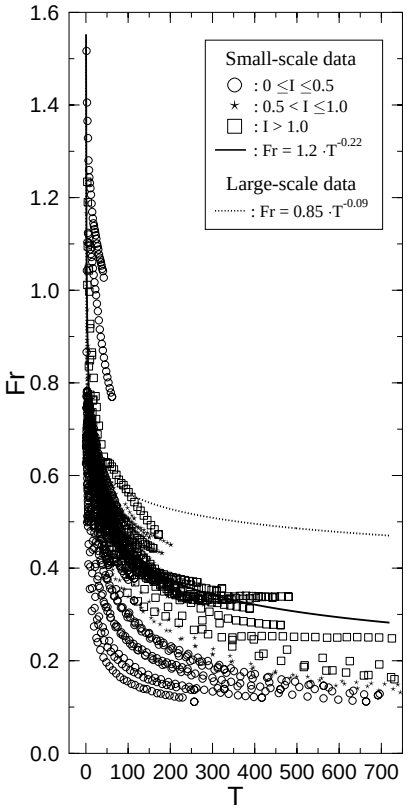

Figure 8: Fr *vs.* T; Small-scale data.

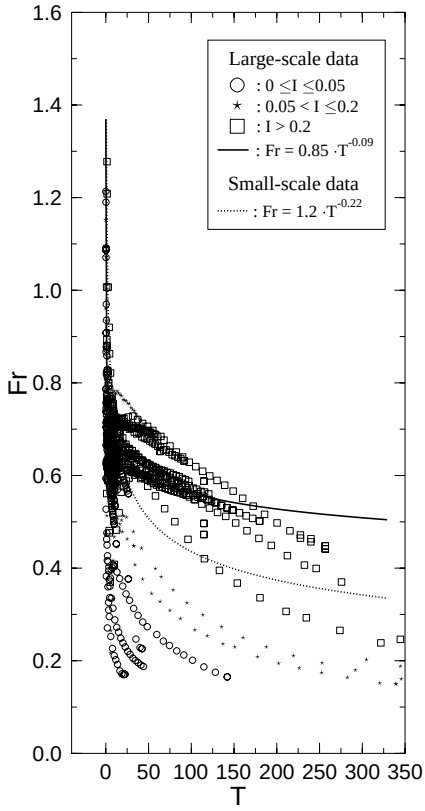

Figure 9: Fr *vs.* T; Large-scale data.

trend for the Froude number to adopt lower values for smaller values of I. Low values of I correspond to high values of the Ekman number (see **?**) and, hence, to the parameter regime where viscous effects become increasingly important and where our inviscid model is no longer valid.

For the vast majority of all data points for highest values of I (lowest Ek), the Froude number lies within the interval $0.35 \leq Fr \leq 0.78$. The solid lines, given by $Fr = 0.85T^{-0.09}$ and $Fr = 1.2T^{-0.22}$, interpolating the data points in Figs. 8 and 9 were determined by plotting all data in double-logarithmic representation and then fitting lines through the regions displaying highest concentrations of data points by eye. These lines are rough guidelines summarizing the data behaviour for the higher values of the parameter I; they do *not* represent least-squares fits. To facilitate easy intercomparison, the solid line of Fig. 8 corresponds to the dotted line in Fig. 9 and *vice versa*. The two figures show that most data lie within $0.35 \leq Fr \leq 0.78$. This is in overall good agreement with our model which predicts $Fr = 0.5303$. For a comparison with corresponding Froude number values found by other authors, refer to **?**.

6 Conclusions

We compared theoretical predictions of a new geostrophic model for gravity-driven coastal surface currents to experimental data. Experiment and model are, generally, in good agreement. A detailed summary and discussion of our results is available in **?**.

Our present model only describes currents flowing along vertical boundaries. We have recently begun to investigate the more realistic scenario where the currents flow along sloping coastlines. To this end, we are currently preparing an experimental study funded through the

EU's HYDRALAB III initiative. This study will be conducted in May 2007 employing the 5m-diameter Coriolis tank of the *Marine Systems Research Infrastructure* (www.ntnu.no/trondheim-marine-RI).

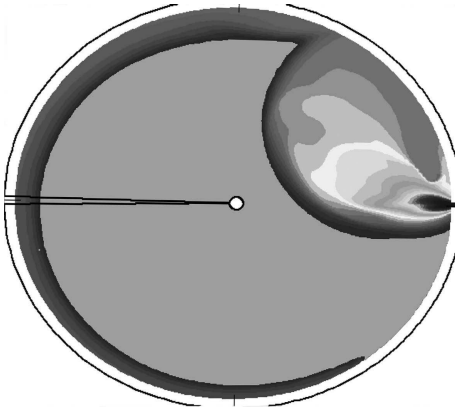

Figure 10: Visualization of a current from our computational simulations.

In collaboration with our colleagues from the *Institute of Marine and Coastal Sciences (IMCS)* at Rutgers University, we are currently also initiating numerical simulations of the flow. While we do not yet have data available that lend themselves to a quantitative comparison with our experiments, we already obtained some first preliminary computational results. One typical current simulated with Rutgers' ROMS code (www.myroms.org) is shown in Fig. 10 ($\Omega = 0.5$ rads^{-1}, $g' = 86.3$ cms^{-2}, $q_0 = 20.0$ cm^{3}s^{-1}, $I = 0.063$ at $t = 30$ s). A comparison of Fig. 10 with the photograph in Fig. 3 already reveals promising qualitative agreement.

References

Avicola, G. & Huq, P. 2002 Scaling analysis for the interaction between a buoyant coastal current and the continental shelf: Experiments and observations. *J. Phys. Oceanography* **32**, 3233-3248.

Davies, P. A., Jacobs, P. T. & Mofor, L. A. 1993 A laboratory study of buoyant fresh water boundary currents in tidal crossflows. *Oceanologica Acta* **16**, 489-503.

Griffiths, R. W. 1986 Gravity currents in rotating systems. *Ann. Rev. Fluid Mech.* **18**, 59-89.

Lentz, S. J. & Helfrich, K. R. 2002 Buoyant gravity currents along a sloping bottom in a rotating fluid. *J. Fluid Mech.* **464**, 251-278.

Thomas, P.J., Linden, P.F. 2007 Rotating Gravity Currents: Small-scale and large-scale experiments and a geostrophic model. In print: *J. Fluid Mech.*.